J Therm Anal Calorim (2011) 103:435–441
DOI 10.1007/s10973-010-0928-0

Thermal and SO_2 adsorption properties of some clays from Turkey

Meryem Sakizci · Burcu Erdoğan Alver · Ertuğrul Yörükoğullari

Received: 29 March 2010 / Accepted: 11 June 2010 / Published online: 7 July 2010

Abstract Thermal and structural properties of three clays (sepiolite and two kaolinites) from Turkey were studied by thermal analysis (TG–DTA), X-ray diffraction (XRD), X-ray fluorescence (XRF), Fourier transform infrared (FT-IR), and surface area measurement techniques The adsorption of sulfur dioxide (SO_2) gas by these clays was also investigated. SO_2 adsorption values of K1, K2, and S clay samples were measured at 20 °C and pressures up to 106 kPa. Sepiolite sample (S) primarily consists of pure sepiolite, only dolomite present as accompanying mineral. Both kaolinite samples, K1 and K2, mainly contain kaolinite as the major clay mineral and quartz as impurity. In K2 sample, muscovite phase is also present. Simultaneous TG–DTA curves of all clay samples were obtained at three different heating rates 10, 15, and 20 °C min^{-1} over the temperature range 30–1200 °C. It was found that the retention value of SO_2 by S clay (2.744 mmol/g) was higher than those of K1 (0.144 mmol/g) and K2 (0.164 mmol/g) samples.

Keywords Adsorption · Clays · DTA · FT-IR · SO_2 · Thermal properties

Introduction

Clays are hydrous aluminosilicates of colloidal dimensions (2 μm) and are the product of the weathering of rocks [1].

M. Sakizci (✉) · B. Erdoğan Alver · E. Yörükoğullari
Department of Physics, Science Faculty, Anadolu University, 26470 Eskisehir, Turkey
e-mail: msakizci@anadolu.edu.tr

Sepiolite is a fibrous clay mineral having tetrahedral and octahedral sheets of oxides. The structural formula of sepiolite is $Si_{12}O_{30}Mg_8(OH)_4(H_2O)_4.8H_2O$. It has fine microporous channels of dimensions 3.7 × 10.6 Å running parallel to the fiber axis [2]. Due to these channels, sepiolite is an important sorbent for many vapors and gases [3–7]. These structural characteristics of sepiolite are account for its high surface area and the capacity. BET surface area of sepiolite for N_2 gas generally ranges between 230 and 380 m^2/g, also depends on deposit and history of the mineral [8]. Fibrous sepiolite mineral has various industrial applications requiring high resistance to thermal effects in addition to a high surface area. Henceforth, the investigation of thermal behavior and determination of surface area of sepiolite mineral has a great importance.

Kaolinite is one of the most abundant clay minerals. Kaolinite is a layered aluminosilicate with a dioctahedral 1:1 layer structure consisting of an octahedral aluminum hydroxide sheet and silica tetrahedral sheet that share a common plane of oxygen atoms [9, 10]. The ideal formula of kaolinite is $Al_2Si_2O_5(OH)_4$, but in most kaolinite clays there are defects due to isomorphous substitution of Si by Al and other small atoms. Kaolinite clays are widely used in many industrial applications like ceramic, porcelain, food, paint, medicine, cosmetic, chemical, and paper industries, etc. [11, 12]. Knowledge of the structural, surface and adsorption properties of kaolinite is required for optimizing the above-mentioned applications.

SO_2 is one of the air pollutant mainly produced from combustion of fossil fuels and causes adverse effects on human health and the environment. SO_2 is the primary cause of acid rain which damages crops, forests, animals, freshwaters and buildings. Therefore, the reduction of SO_2 emissions is of great importance. There are many papers about adsorption of SO_2 by bentonitic clay minerals

[13–16]. Nevertheless, there is scarce information about the retention of SO_2 by kaolinites and sepiolites [3, 17, 18]. Thermal and structural analyses are widely used in the study of properties of sepiolite and kaolinite samples [19–32]. There are large sepiolite and kaolinite reserves in different regions of Turkey. However, there has not been enough study about the thermal, structural, and SO_2 adsorption properties of Turkey clays. The main objective of this study is to investigate three clay samples in terms of their clay types, chemical compositions, thermal, structural, and SO_2 adsorption properties.

Experimental

Material

The sepiolite sample named 'S' was obtained from Sivrihisar, Turkey. The kaolinite samples labeled as 'K1' and 'K2' were obtained from Kütahya and Bilecik regions, respectively. The samples were air dried at room temperature and ground to pass through a <100 μm sieve.

Instrumentation

The XRD diffractograms were obtained with a Rigaku RINT-2200 instrument, using CuKα radiation ($\lambda = 1.54$ Å) at 40 kV and 20 mA, in the range 3–40° 2θ. The samples were scanned with a step of 0.02° 2θ. The chemical analyses of clay samples were carried out using a Rigaku ZSX Primus model XRF instrument. Infrared spectra of the clay samples were recorded in the region of (4000–400) cm^{-1} via Perkin-Elmer FT-IR spectrum 2000 spectrometer at a resolution of 4 cm^{-1} using KBr pellet technique.

The BET surface areas of the samples were measured with volumetric sorption analyzer (NOVA 2200, Quantachrome Instruments, USA) using nitrogen gas adsorption at −196 °C. Before each measurement, the samples were degassed at 125 °C for 6 h. High purity (99.99%) nitrogen was used as the adsorbate.

Simultaneous TG–DTA experiments were carried out using a Setsys Evolution Setaram thermal analyzer. Approximately, 25 mg of sample was used in each run. Powdered samples were loaded into alumina pan. The empty alumina pan was used as reference. All experiments were performed at the heating rates of 10, 15, and 20 °C min^{-1} over the temperature range of 30–1200 °C.

Retention values of SO_2 by clay samples were determined using automated volumetric equipment (Autosorb 1-Quantachrome Instruments, USA) at 20 °C. About 0.2 g of the sample was outgassed in vacuum at 125 °C for 7 h before sulfur dioxide adsorption.

Results and discussion

Characterization of sepiolite and kaolinite clays

Three local samples were investigated through chemical analysis. The chemical analysis of clay samples was carried out and the data were presented in Table 1. Na_2O, K_2O, Fe_2O_3, and TiO_2 are present only very small amounts in sepiolite sample. The MgO content of sepiolite-rich sample is 18.98% and the SiO_2 content is 46.28%. The theoretical SiO_2/MgO ratio of sepiolite is 2.23 and SiO_2 is typically on the order of 55.9 ± 1.9% and MgO 21–25% [33]. The SiO_2/MgO ratio of sepiolite used this study is 2.43 and this ratio is similar to ideal sepiolite [34] whereas it is greater than theoretical ratio of sepiolite. Furthermore, the SiO_2 and MgO contents are less than the theoretical ratio of sepiolite. The differences in chemical composition reflect the mineralogy of the sediments. The MgO comes both from sepiolite and dolomite. The CaO is originated only from dolomite. The LOI is due to the dehydration and dehydroxylation of the sepiolite and also calcination of the dolomite.

Comparison between the chemical composition of K1 and K2 clays and ideal composition of kaolinite shows that these samples have higher SiO_2 contents [35]. Loss on ignition (LOI) values of the kaolinite samples is similar (Table 1). The excess of SiO_2 is due to the presence of quartz, as shown by XRD [36]. K1 clay sample contains a lower content of Fe_2O_3, TiO_2, K_2O and MgO compared with the K2 clay sample.

X-ray diffraction

The XRD patterns of the clay samples are shown in Fig. 1. It can be seen from Fig. 1 that the main impurity in the sepiolite was dolomite. Therefore, the natural rock contains sepiolite and dolomite as clay and nonclay minerals,

Table 1 Chemical compositions of the clay samples in wt%

Chemical analysis/%	K1	K2	Ideal kaolin [35]	S
SiO_2	69.18	61.86	46.55	46.28
Al_2O_3	21.74	24.52	39.49	4.77
Fe_2O_3	0.32	1.11	–	2.02
CaO	0.08	0.06	–	2.87
MgO	–	0.28	–	18.98
Na_2O	0.05	0.08	–	0.15
K_2O	0.06	2.31	–	0.45
TiO_2	0.43	1.47	–	0.29
P_2O_5	0.12	0.08	–	0.01
Others	0.22	0.17	–	0.33
LOI	7.80	8.06	13.96	23.85

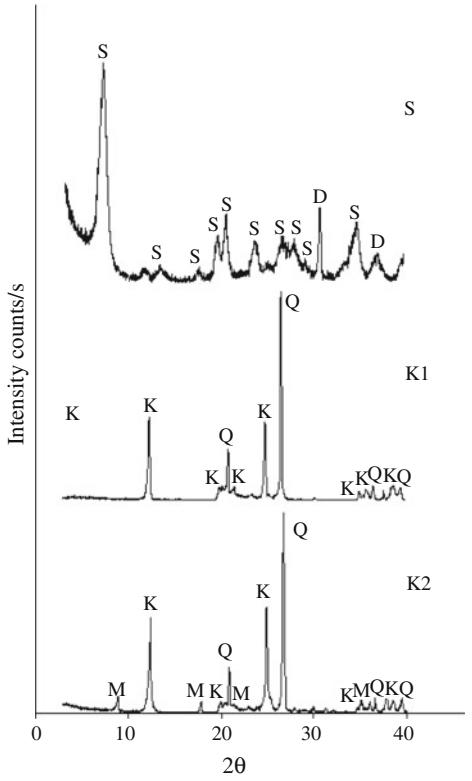

Fig. 1 X-ray diffraction pattern of the S, K1 and K2 samples (*S* sepiolite, *D* dolomite, *K* kaolinite, *Q* quartz, *M* muscovite)

respectively. The XRD pattern of the sepiolite sample shows the characteristic (110) reflection of sepiolite at 12.4 Å. This value is slightly greater than those reported in the literature [37, 38]. Other moderate-intensity reflections for sepiolite are at 4.5, 4.3, 3.74, 3.34, 3.17, and 2.57 Å. Dolomite peaks at 2.90 and 2.41 Å were observed in XRD analysis.

The XRD pattern of the K1 clay (Fig. 1) contained kaolinite as the principal mineral (characteristic peaks at 7.18 and 3.58 Å) with quartz (peaks 4.26, 3.35, and 2.28 Å). The XRD pattern of the K2 clay (Fig. 1) contained kaolinite as the major mineral (characteristic peaks 7.12 and 3.56 Å), with muscovite (characteristic peaks 9.92 and 4.96 Å) and quartz (characteristic peaks 4.24, 3.33, and 2.27 Å). The basal spacing of the K1 sample (7.18 Å) is slightly greater than that of the K2 sample (7.12 Å).

Specific surface area

BET evaluation ($P/P_o = 0.05$–0.35) was used to measure specific surface areas of the clay samples [39, 40]. Applications of BET model give the specific surface areas of 324, 6.6, and 7.5 m^2/g for S, K1 and K2 samples, respectively (Table 2). Both kaolinite samples exhibit a very low specific surface area. The surface area values of K1 and K2

Table 2 BET surface area values and SO_2 retentions of clay samples

Samples	$S_{BET}/m^2\ g^{-1}$	$SO_2/mmol\ g^{-1}$
K1	6.6	0.144
K2	7.5	0.164
S	324	2.744

samples are in agreement with those generally determined (10–30 m^2/g) for kaolinite-type materials [41].

FT-IR studies

FT-IR spectra of S, K1 and K2 samples are shown in Fig. 2. In the FT-IR spectrum of S sample, the bands at ~3689, 3623, 3568, 3432, and 3252 cm^{-1} are attributed to

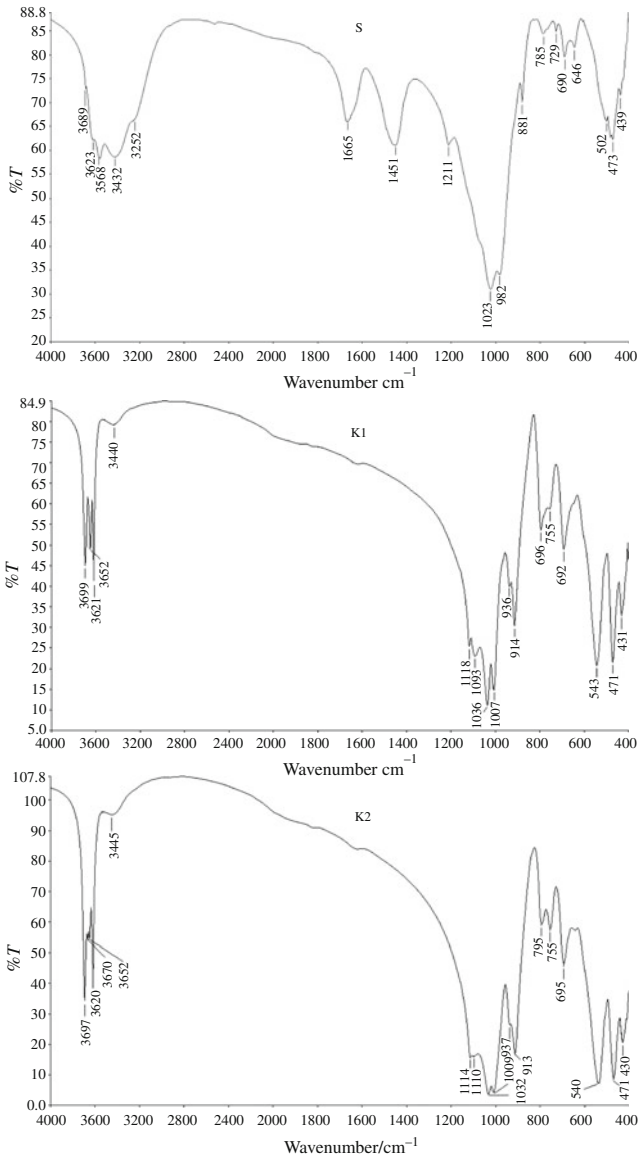

Fig. 2 FT-IR spectra of S, K1, and K2 samples

the presence of adsorbed and zeolitic water molecules in the structure of mineral [24, 25]. The band at 3432 and 1665 cm^{-1} are due to OH stretching and bending of water molecules, respectively (zeolitic or interior or channel water) [42]. The band at 1451 cm^{-1} is attributed to the dolomite impurity [24]. The band at 1211 cm^{-1} is due to Si–O–Si bond [43]. The bands corresponding to the in plane Si–O–Si vibrations are observed at 1023, 982, and 473 cm^{-1} [44]. The bands at ~785, 690, and 646 cm^{-1} are assigned to inner Mg–OH bending vibrations. In addition, the band at 439 cm^{-1} is due to Si–O–Mg bonds [24, 45].

In the FT-IR spectrum of K1 sample, the bands at 3699, 3652, and 3621 cm^{-1} are characteristic ν_{OH} vibrations for kaolinite. The bands at 1118, 1093, 1036, and 1007 cm^{-1} are due to Si–O vibrations [27, 46]. OH deformation bands appear at 936 and 914 cm^{-1}. The bands at 796 and 755 cm^{-1} are attributed to the Si–O–Si vibrations. The band at 543 cm^{-1} is assigned to Si–O vibrations. In the FT-IR spectrum of K2 sample, four bands appear at 3697, 3670, 3652, and 3620 cm^{-1} are typical OH strecthing bands for kaolinite [27]. The vibrations of Si–O groups are observed at 1114, 1110, 1032, and 1009 cm^{-1}. The bands appear at 937 and 913 cm^{-1} are due to the OH deformation. The bands at 795 and 755 cm^{-1} are assigned to Si–O–Si vibrations, while the band at ~540 cm^{-1} is due to Si–O–Al bending vibrations [27]. In addition, the vibrations of Si–O groups appear around 695, 471 and 430 cm^{-1} [46].

Thermal properties

The clay samples in order to see the effect of the heating rate were heated at 10, 15, and 20 °C min^{-1}, up to a temperature in the 30–1200 °C range. Temperature intervals and peak temperatures of the clay samples are given in Table 3. DTA-TG curves of the clay samples are given in the Figs. 3, 4, and 5. Six endothermic changes and one exothermic change for sepiolite are seen at heating rate 10 °C min^{-1} in the DTA curve (Fig. 3). The first and dominant endothermic mass loss of 6.23% in the temperature range of 30–250 °C with the maximum rates at 110 and 210 °C are due to the dehydration of hydroscopic water and zeolitic water. The second endothermic mass loss of 2.18% between 250 and 365 °C with the maximum rate at 303 °C is due to the dehydration rest part of zeolitic water and the first part of the bound water. The total of mass losses up to 365 °C is 8.41%. The third endothermic mass loss of 3.29% in the temperature range of 365 and 570 °C with the maximum rate at 429 °C is attributed to the dehydration of the second part of the bound water. The calcination of the dolomite and dehydroxylation of the sepiolite give rise to fourth and fifth endothermic mass losses of 6.13% after 570 °C up to 1200 °C with the maximum rates at 732 and 812 °C. An exothermic peak at 840 °C is sharp, beginning at 825 °C and ending at 887 °C. The crystal structure of sepiolite has collapsed in this last reaction. The dehydration of the present sepiolite is in good agreement with those of the sepiolite described by other authors [26, 29, 47, 48]. For sepiolite sample, the mass loss during thermal decomposition is 16.11% at 750 °C and 17.83% at 1200 °C.

Table 3 TG–DTA data of S, K1 and K2 samples

Sample	Heating rate/°C min^{-1}	Temp. interval/°C	End. peak/°C	Exo. peak/°C
S	10	30–250	110, 210	
		250–365	303	
		365–570	429	
		570–1200	732,812	840
	15	30–250	122, 218	
		250–400	307	
		400–570	441	
		570–1200	743,819	845
	20	30–300	132, 248	
		300–400	343	
		400–570	445	
		570–1200	755,831	852
K1	10	30–400	89, 173, 234	
		400–1200	531, 671	1012
	15	30–400	111, 215, 300	
		400–1200	552, 678	1016
	20	30–400	133, 253, 351	
		400–1200	580, 688	1020
K2	10	30–400	86, 172, 241	
		400–1200	525	1008
	15	30–400	105, 209, 297	
		400–1200	539	1014
	20	30–400	128, 247, 343	
		400–1200	548	1017

The TG–DTA curves of the kaolinite samples are similar (Figs. 4, 5). The DTA curve of the K1 sample at heating rate 10 °C min^{-1} exhibits three endothermic peaks at 89, 173, and 234 °C in the range of 30–400 °C temperature ranges. These peaks corresponded to the removal of adsorbed and interlayer water. The elimination of the structural hydroxyls of the octahedral sheet gives rise to endothermic peaks at 531 and 671 °C. Intense exothermic peak at 1012 °C is attributed to the formation of a spinal phase [49–51].

The evaluation of adsorbed and interlayer water from K2 is presented by three endothermic peaks at 86, 172, and 241 °C in the DTA curve at heating rate 10 °C min^{-1}. Fourth endothermic peak between 415 and 670 °C with the maximum rate at 525 °C corresponds to the

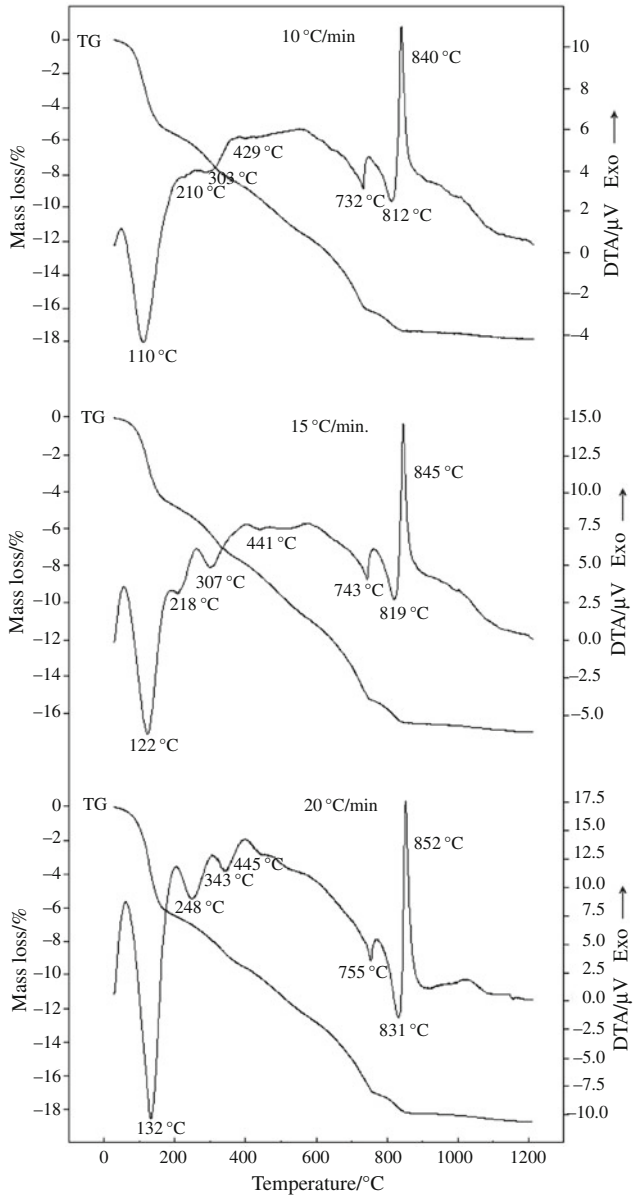

Fig. 3 TG and DTA curves for the S sample

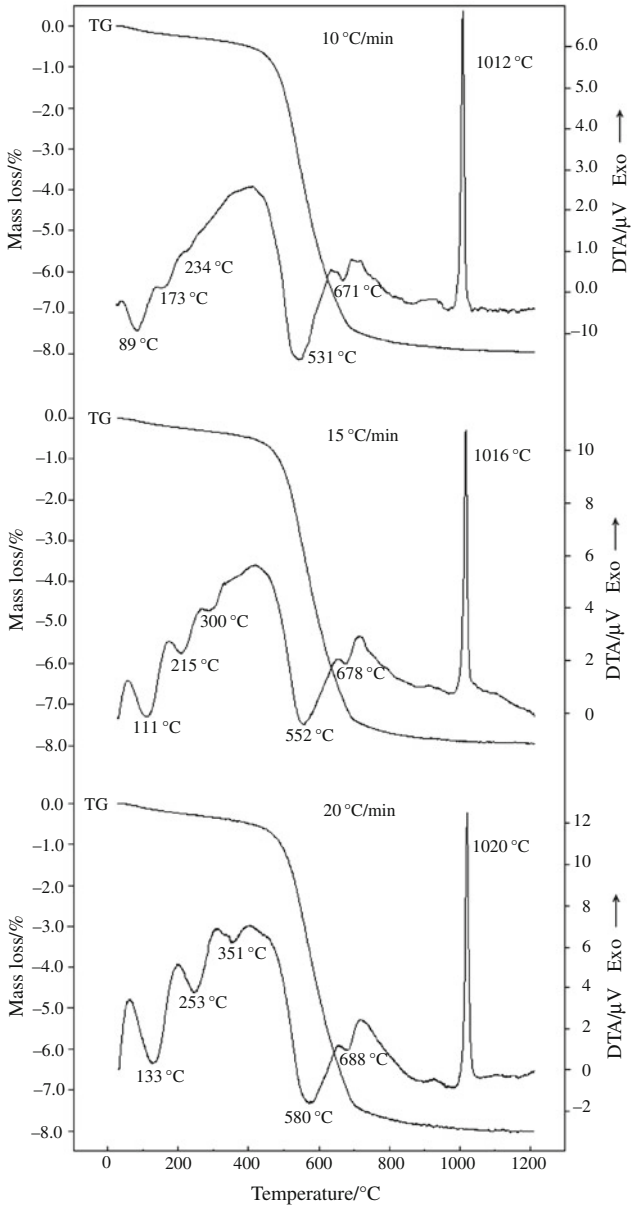

Fig. 4 TG and DTA curves for the K1 sample

dehydroxylation process to metakaolinite [52, 53]. In addition, the formation of a spinel phase results in a sharp exothermic DTA peak at 1008 °C.

Mass changes of the K1 and K2 samples studied plotted as a function of temperature are shown in Figs. 4 and 5. The TG curves for both samples exhibit a similar two-step weight loss. The first step (starting at 30 °C) corresponds to the elimination of physically adsorbed water and interlayer water. The second one (starting at 400 °C) reflects the loss of structurally bonded water. The total mass losses of K1 and K2 were determined as 7.8 and 7.9%, respectively.

It was observed that different heating rates influenced the intensities of both endothermic and exothermic peaks related to the dehydration, dehydroxylation, and then crystallization of a new phase (Table 3; Figs. 3, 4, 5). Higher peak temperatures are obtained with increasing heating rate.

Gas adsorption

Adsorption processes are of great importance for removal of pollutants. Sulfur dioxide (SO_2) adsorption of K1, K2, and S clay samples was measured using a volumetric apparatus, at 20 °C and pressures up to 106 kPa. High purity SO_2 gas was used as the adsorbate. The absolute amounts adsorbed per gram of clay samples are given in Table 2. A relationship was found between gas adsorption and the BET surface area. A large specific surface area is preferable for providing a

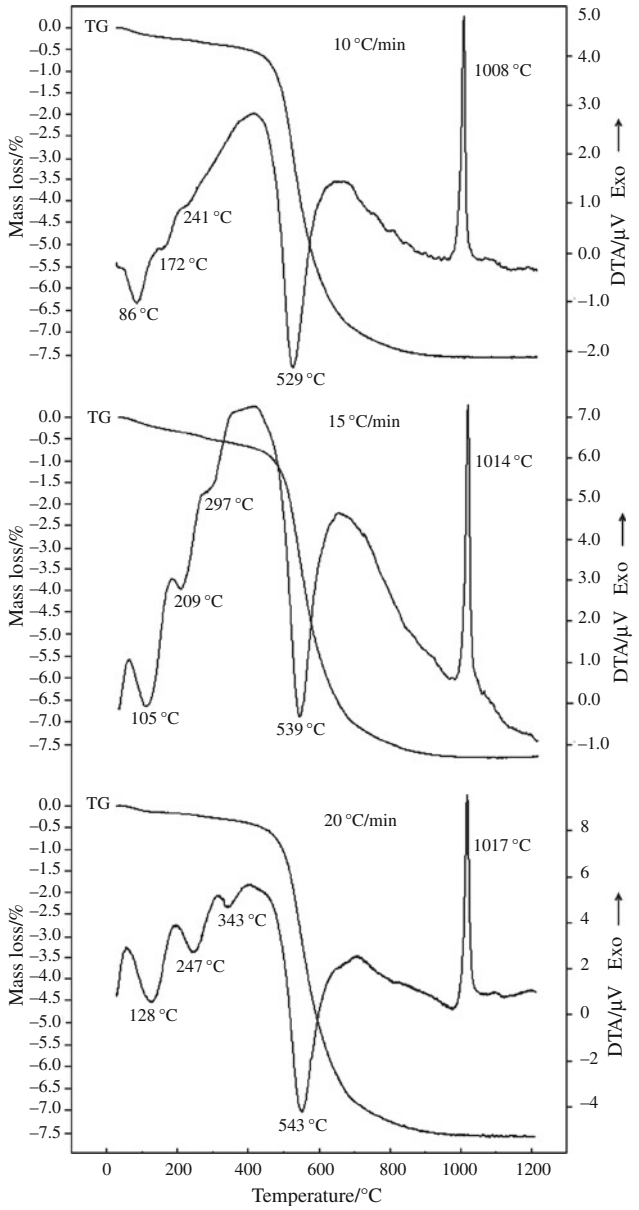

Fig. 5 TG and DTA curves for the K2 sample

large adsorption capacity depending on clay mineral. Sepiolite (S) showed much higher SO_2 adsorption (2.744 mmol/g) than K1 (0.144 mmol/g) and K2 (0.164 mmol/g) samples. The retention values of SO_2 by K1 and K2 samples in this paper were lower than those of kaolinite samples (0.201–0.542 mmol/g [17]).

The presence of impurities as quartz in kaolinites may affect the retention of gases because the adsorption of these minerals is usually small [18, 54]. SO_2 gas retention in K2 clay was higher than that of K1 clay. It could be attributed to a larger amount of clay components in K2 clay. The results indicate that S has good performance in SO_2 removal compared with K1 and K2 samples.

Conclusions

In present work, clay samples were characterized using XRD, XRF, FT-IR, TG–DTA and surface area measurement methods. Adsorptions of SO_2 on clay samples have been obtained at 20 °C pressures up to 106 kPa. Both the mineral and chemical purities of the powder samples were established. The K1 and K2 clay samples contain kaolinite as the major clay mineral and also quartz as impurity. In K2 sample, muscovite phase is also present.

The temperature ranges were determined for the dehydrations of hydroscopic and zeolitic water as 30–250 °C, for the dehydration of the bound water as 250–750 °C and dehydroxylation of hydroxyls as 810–850 °C in TG–DTA curve of S sample. The thermal behavior is similar in shape for kaolinite clays. It was determined that the DTA curves of K1 and K2 clay samples showed three endothermic peaks between 30–300 °C corresponding to the loss of adsorbed and interlayer water. The endothermic peak between 400–685 °C corresponded to the loss of the structural OH of kaolinite and associated with kaolinite–metakaolinite phase transition. The exothermic peak observed at around 1000 °C for K1 and K2 was related to the formation of a spinel phase. It was also observed that the heating rate employed in TG–DTA analysis significantly effects peak temperatures. The effects of high heating rate give rise to the reactions to occur at higher temperatures.

It was found that SO_2 adsorption capacity of S sample was much greater than K1 and K2 samples. In conclusion, compared with K1 and K2 samples, S sample could be proposed as an adsorbent for removing SO_2 from contaminated environments.

References

1. Rouquerol F, Rouquerol J, Sing K. Adsorption of powders and porous solids principles, methodology and applications. USA: Academic Press; 1999.
2. Brauner K, Preisinger A. Struktur und Entstehung des Sepioliths. Tschermaks Miner. Petr. Mitt. 1956;6:120–40.
3. Matsuda T, Ikeya M. Thermal stability of SO_2- and NO_2 adsorbed on the surface of sepiolite, a porous clay mineral. Jpn J Appl Phys. 2002;41:2916–9.
4. Shuali U, Yariv S, Steinberg M, Muller Vonmoos M, Kahr G, Rub A. Thermal analysis study of the adsorption of D_2O by sepiolite and palygorskite. Thermochim Acta. 1988;135:291–7.
5. Tosi-Pellenq N, Grillet Y, Rouquerol J, Llewellyn P. A microcalorimetric comparison of the adsorption of various gases on two microporous adsorbents: a model aluminophosphate and a natural clay. Thermochim Acta. 1992;204:79–88.
6. Erdoğan Alver B, Sakizci M, Yörükoğulları E, Yılmaz Y, Güven M. Thermal behavior and water adsorption of natural and modified sepiolite having dolomite from Turkey. J Therm Anal Calorim. 2008;94:835–40.
7. Molina-Sabio M, Caturla F, Rodríguez-Reinoso F, Kharitonova GV. Porous structure of sepiolite as deduced from the adsorption

of N_2, CO_2, NH_3 and H_2O. Micropor Mesopor Mater. 2001;47: 389–96.
8. Galan E. Properties and applications of palygorskite-sepiolite clay. Clays Clay Miner. 1996;31:443–53.
9. Bear FE. Chemistry of soil. 2nd ed. New York: Reinhold Publishing; 1965.
10. Srivastava P, Singh B, Angove M. Competitive adsorption behavior of heavy metals on kaolinite. J Colloid Interface Sci. 2005;290:28–38.
11. Murray HH. Applied clay mineralogy today and tomorrow. Clay Miner. 1999;34:39–49.
12. Murray HH. Traditional and new applications for kaolin, smectite, and palygorskite: a general overview. Appl Clay Sci. 2000;17: 207–21.
13. Venaruzzo JL, Volzone C, Rueda ML, Ortiga J. Modified bentonitic clay minerals as adsorbents of CO, CO_2 and SO_2 gases. Micropor Mesopor Mater. 2002;56:73–80.
14. Volzone C, Rinaldi JO, Ortiga J. Retention of gases by hexadecyltrimethylammonium-montmorillonite clays. J Environ Manage. 2006;79:247–52.
15. Volzone C. Retention of pollutant gases: comparison between clay minerals and their modified products. Appl Clay Sci. 2007; 36:191–6.
16. Volzone C, Ortiga J. Adsorption of gaseous SO_2 and structural changes of montmorillonite. Appl Clay Sci. 2009;44:251–4.
17. Volzone C, Ortiga J. Removal of gases by thermal-acid leached kaolinitic clays: influence of mineralogical composition. Appl Clay Sci. 2006;32:87–93.
18. Melnitchenko A, Thompson JG, Volzone C, Ortiga J. Selective gas adsorption by metal exchanged amorphous kaolinite derivative. Appl Clay Sci. 2000;17:35–53.
19. Felhi M, Tlili A, Gaied ME, Montacer M. Mineralogical study of kaolinitic clays from Sidi El Bader in the far north of Tunisia. Appl Clay Sci. 2008;39:208–17.
20. Sweeney M. A mineralogical study of some West Indian soil-clays. Thermochim Acta. 1981;48:323–31.
21. Yeniyol M. Vein-like sepiolite occurrence as a replacement of magnesite in Konya, Turkey. Clays Clay Miner. 1986;34:353–6.
22. Chakraborty AK. New data on thermal effects of kaolinite in the high temperature region. J Therm Anal Calorim. 2003;71:799–808.
23. Souaya RE, Selim SA, Tobia SK. Thermal and spectroscopic investigations of some Egyptian clays. Thermochim Acta. 1983;65:359–74.
24. Perraki Th, Orfanoudaki A. Study of raw and thermally treated sepiolite from the Mantoudi area, Euboea, Greece. J Therm Anal Calorim. 2008;91:589–93.
25. Frost RL, Locos OB, Ruan H, Kloprogge JT. Near-infrared and mid-infrared spectroscopic study of sepiolites and palygorskites. Vib Spectrosc. 2001;27:1–13.
26. Chakraborty AK. DTA study of preheated kaolinite in the mullite formation region. Thermochim Acta. 2003;398:203–9.
27. Saikia NJ, Bharali DJ, Sengupta P, Bordoloi D, Goswamee RL, Saikia PC, Borthakur PC. Characterization, beneficiation and utilization of a kaolinite clay from Assam, India. Appl Clay Sci. 2003;24:93–103.
28. Frost RL, Ding Z. Controlled rate thermal analysis and differential scanning calorimetry of sepiolites and palygorskites. Thermochim Acta. 2003;397:119–28.
29. Nagata H, Shimoda S, Sudo T. On dehydration of bound water of sepiolite. Clays Clay Miner. 1974;22:285–93.
30. Castelein O, Soulestin B, Bonnet JP, Blanchart P. The influence of heating rate on the thermal behaviour and mullite formation from a kaolin raw material. Ceram Int. 2001;27:517–22.
31. Ibrahim DM, Kabish AM, Ghoneim N. Thermal behaviour of some raw materials and ceramic mixes. Thermochim Acta. 1984; 75:43–50.
32. Kristof J, Frost RL, Kloprogge JT, Horvath E, Mako E. Detection of four different OH groups in ground kaolinite with controlled-rate thermal analysis. J Therm Anal Calorim. 2002;69:77–83.
33. Jones BF, Galan E. Sepiolite and Palygorskite. In: Bailey SW, editor. Hydrous phyllosilicates:mineralogical society of america reviews in mineralogy. Washington, DC: Mineralogical Society of America; 1988. p. 631–74.
34. Weaver CE. Clays, muds and shales. Developments in sedimentology. Amsterdam: Elsevier; 1989.
35. Newman ACD. Chemistry of clays and clays minerals. In: Newman ACD, editor. The chemical constitution of clays, mineralogical society monograph. London: Longmans; 1987. p. 2–128.
36. Grimshaw RW. Physics and chemistry of clay. 4th ed. London: Ernest Benn; 1971.
37. Bailey SW. Structures of layer silicates. In: Brindley GW, Brown G, editors. Crystal structures of clay minerals and their x-ray identifications. London: Mineralogical Society; 1980. p. 2–123.
38. Grim RE. Clay mineralogy. New York: McGraw-Hill; 1953.
39. Brunauer S, Emmett PH, Teller E. Adsorption of gases in multimolecular layers. J Am Chem Soc. 1932;60:309–19.
40. Gregg SJ, Sing KSW. Adsorption, surface area and porosity. London: Academic Press; 1991.
41. Guyot J. Mesure des surfaces spécifiques des argiles par adsorption. Ann Agronomiques. 1969;20:333–59.
42. Casal B, Merino J, Serratosa J, Ruiz-Hitzky E. Sepiolite-based materials for the photo- and thermal-stabilization of pestisites. Appl Clay Sci. 2001;18:245–54.
43. Torró-Palau A, Fernández-García J, Orgilés-Barceló AC, Mercedes Pastor-Blas M, Martín-Martínez J. Structural modification of sepiolite (natural magnesium silicate) by thermal treatment: effect on the properties of polyurethane adhesives. Int J Adhes Adhes. 1997;17:111–9.
44. Vicente-Rodriguez M, Suarez M, Banares-Munoz M, Lopez-Gonzalez J. Comparative FT-IR study of the removal of octahedral cations and structural modifications during acid treatment of several silicates. Spectrochim Acta. 1996;52A:1685–94.
45. Prost R. Infrared study of the interactions between the different kinds of water molecules present in sepiolite. Spectrochim Acta. 1975;31A:1497–9.
46. Guimaraes JL, Peralta-Zamora P, Wypych F. Covalent grafting of phenylphosphonate groups onto the interlamellar aluminol surface of kaolinite. J Colloid Interface Sci. 1998;206:281–7.
47. Kiyohiro T, Otsuka R. Dehydration mechanism of bound water in sepiolite. Thermochim Acta. 1989;147:127–38.
48. Serna C, Ahlrichs JL, Serratosa JM. Folding in sepiolite crystals. Clays Clay Miner. 1975;23:452–7.
49. Okada K, Ostuka N, Ossaka J. Characterization of spinel phase formed in the kaolin-mullite thermal sequence. J Am Ceram Soc. 1986;69:251–3.
50. Gualtieri A, Bellotto M, Artioli G, Clark SM. Kinetic study of the kaolinite-mullite reaction sequence. Part II: mullite formation. Phys Chem Miner. 1995;22:215–22.
51. Srikrishna K, Thomas G, Martinez R, Corral MP, De Aza S, Moya JS. Kaolinite-mullite reaction series: a TEM study. J Mater Sci. 1990;25:607–12.
52. Toussaint J, Fripiat J, Gastuche MC. Dehydroxylation of kaolinite. I. Kinetics. J Phys Chem. 1963;67:26–30.
53. Ortega A, Rouquerol F, Akhouayri S, Laureiro Y, Rouquerol J. Kinetical study of the thermolysis of kaolinite between −30 and 1000 °C by controlled rate evolved gas analysis. Appl Clay Sci. 1993;8:207–14.
54. Volzone C, Thompson JG, Melnitchenko A, Ortigaand J, Palethorpe SR. Selective gas adsorption by amorphous clay mineral derivative. Clays Clay Miner. 1999;47:647–57.